Journal of Fiber Bioengineering and Informatics 8:3 (2015) 521–528
doi:10.3993/jfbim00125

An Iterative Image Reconstruction for Differential X-ray Phase-contrast Computed Tomography ⋆

Fengrong Sun [a,b], Paul Babyn [b,*], Tetsuya Yuasa [c], Mingqiang Zhang [d]
Feng Qin [a], Naoki Sunaguchi [e], Khan A. Wahid [f], Masami Ando [g]

[a] *School of Information Science and Engineering, Shandong University, Jinan 250100, China*
[b] *Department of Medical Imaging, University of Saskatchewan, Saskatoon, Canada*
[c] *Yamagata University, 4-3-16 Jonan, Yonezawa, 992-8510 Japan*
[d] *College of Physics and Engineering, Qufu Normal University, Qufu 273165, China*
[e] *Graduate School of Engineering, Gunma University, Japan*
[f] *Department of Electrical and Computer Engineering, University of Saskatchewan, Saskatoon, Canada*
[g] *Research Institute for Science and Technology, Tokyo University of Science, Japan*

Abstract

The last decade saw the growth of the use of X-ray Phase-contrast Computed Tomography (PCT) imaging. Differential X-ray Phase-contrast CT (DPCT) has shown bright prospect for clinical use in recent years, but how to best reconstruct the phase-contrast tomographic image from incomplete or inconsistent projections remains challenging. We designed an iterative image reconstruction method for DPCT utilizing compressed sensing. This proposed method reconstructs the phase-contrast tomographic image of the refractive index decrement gradient with acceptable accuracy and image quality even when the projection data is undersampled or noisy. Real data experiments indicate this proposed method is accurate and practical and outperforms the analytic filtered back-projection reconstruction. This method shows potential for X-ray DPCT facilities in low dose tomography and fast acquisition imaging.

Keywords: X-ray Phase-contrast Imaging; Computed Tomography (CT); Compressed Sensing; Low Dose Tomography; Fast Acquisition Imaging

1 Introduction

Phase sensitive X-ray imaging, in which additional contrast is generated by the refraction of hard X-rays as they pass through the object under study, can provide substantially increased contrast over conventional absorption-based imaging and new and otherwise inaccessible information [1–3].

⋆Project partly supported by the National Nature Science Foundation of China (No. 61071053) and the Nature Science Foundation of Shandong Province (No. ZR2014FM006).

*Corresponding author.
Email address: paul.babyn.ijcars@gmail.com (Paul Babyn).

1940–8676 / Copyright © 2015 Binary Information Press & Textile Bioengineering and Informatics Society
September 2015

It originates in the real part of the complex refractive index of hard X-rays for light- or medium-density materials is several orders of magnitude higher than its imaginary part which describes its absorption. The tomographic implementation of phase sensitive X-ray imaging, i.e., X-ray Phase-contrast Computed Tomography (PCT), bears tremendous potential for three-dimensional tomographic imaging of soft biological tissue and other specimens whose details exhibit very weak absorption contrast. PCT imaging techniques have seen significant growth recently. And differential X-ray Phase-contrast CT (DPCT) has shown promise for clinical use in medical imaging [4]. However, tomographic image reconstruction from incomplete (e.g., undersampled) or inconsistent (e.g., heavy noisy) projections is needed in DPCT modalities to ensure low dose tomography and faster acquisition. Such reconstruction with acceptable accuracy and image quality is challenging due to the violation of the Nyquist sampling criteria.

Iterative tomographic image reconstructions possess distinct advantages over their analytic counterparts when the projection data is incomplete or inconsistent. But iterative image reconstruction was not employed in modern commercial CT scanners until recently, owing to the prolonged computation time and the large storage requirement. With the rapid development of signal processing and computation technique as well as the fantastic decrease of computer hardware cost, these limitations are not a significant concern any more. We designed an iterative tomographic image reconstruction method for DPCT under the framework of Compressed Sensing (CS) theory [5, 6]. CS has been applied in conventional absorption contrast CT to address some diagnostic imaging issues [7–9], and also emerges recently in phase sensitive X-ray imaging [10, 11]. The previous work are significant, but we believe the exploration of CS-based iterative tomographic image reconstruction for DPCT still remains an open topic and has just begun.

The complex refractive index of X-rays for an object, generally, can be expressed as $n = 1 - \delta + i\beta$, where the refractive index decrement (i.e., δ) determines the phase shift of the X-rays passing through the object, while the absorption term (i.e., β) is correlated with the linear absorption coefficient. Let us denote the spatial distribution of the refractive index decrement as $\delta(x, y)$. Our method, which will be referred to as the RRL1 method in this paper, reconstructs the spatial distribution of the refractive index decrement gradient (i.e., $\nabla\delta = (\partial\delta/\partial x, \partial\delta/\partial y)$) from X-rays refraction angle data. Real data experiments along with the quantitive performance evaluation indicate the RRL1 method is practical and accurate and overperforms the FBP reconstruction. And the RRL1 method offers the potential for DPCT facilities in low dose tomography and fast acquisition imaging, as it is capable of generating phase-contrast tomographic images with satisfactory fidelity even when the projection data is undersampled and noisy.

2 Theory and Method

As illustrated in Fig. 1, we define the refraction angle of a X-ray beam as the angle of the downstream propagation direction relative to the initial one and denote it as θ. Eq. (1) reveals the relationship between the refraction angle θ and the integral of the directional derivative of $\delta(x, y)$ [12]. The directional derivative of $\delta(x, y)$ in Eq. (1) is with respect to $l_\perp$, which is perpendicular to the X-ray beam path l.

$$\theta = \int \frac{\partial \delta(x, y)}{\partial l_\perp} dl \tag{1}$$

According to the geometry diagramed in Fig. 1 and using angle ϕ to depict the direction of the

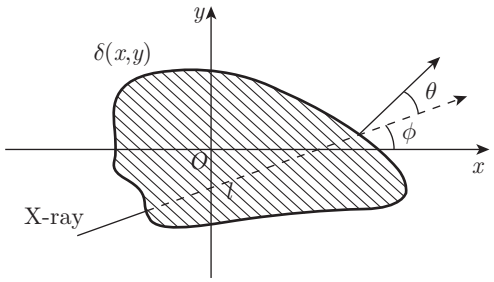

Fig. 1: Illustration of Eq. (1)

incident X-ray beam, we can get Eq. (2) from (1) easily.

$$\theta \sin\phi = \int \frac{\partial \delta\,(x,y)}{\partial x} dl, \qquad \theta \cos\phi = \int \frac{\partial \delta\,(x,y)}{\partial y} dl \tag{2}$$

It means that $\theta \sin\phi$ and $\theta \cos\phi$ are the Radon transforms of $\partial\delta\,(x,y)/\partial x$ and $\partial\delta\,(x,y)/\partial y$ functions respectively. So we can reconstruct the spatial distribution of the refractive index decrement gradient (i.e., $\nabla\delta = (\partial\delta/\partial x, \partial\delta/\partial y)$) from the data set $\left\{(\theta,\phi) \left| \begin{smallmatrix} \theta\text{: the refraction angle} \\ \phi\text{: the direction of the incident } X\text{−ray beam} \end{smallmatrix} \right.\right\}$, either utilizing the analytic FBP method or by an iterative computation scheme. It should be noted that the target phase-contrast image reconstructed by the RRL1 method is $\partial\delta\,(x,y)/\partial x$ or $\partial\delta\,(x,y)/\partial y$, and $\theta \sin\phi$ or $\theta \cos\phi$ is regarded as the projection data.

2.1 CS-based Tomographic Image Reconstruction

CS-based tomographic image reconstruction is, mathematically, realized by solving the following constrained minimization problem:

$$\min_X \|\Psi X\|_{l_1}, \quad s.t.\ \ \Theta X = p \tag{3}$$

where $\|\cdot\|_{\ell_1}$ symbolizes the ℓ_1-norm of a vector, $X \in R^{n\times 1}$ is the vectorized target image and is supposed to be $k-sparse$, the $m-$dimensional column vector p is the measurements $(m << n)$, and the $m \times n$ matrix Θ is defined as $\Theta = \Phi * \Psi$, in which $\Psi \in R^{n\times n}$ is the sparsity basis and $\Phi \in R^{m\times n}$ is the measurement system.

In CT field, the system matrix is used to model the projection of discrete image. We denote it as A and suppose its row vectors having been normalized. (1) RRL1 attempts to recover $\partial\delta\,(x,y)/\partial x$ or $\partial\delta\,(x,y)/\partial y$ from the projection data $\theta \sin\phi$ or $\theta \cos\phi$. $\partial\delta\,(x,y)/\partial x$ or $\partial\delta\,(x,y)/\partial y$ represents the directional edges of $\delta\,(x,y)$ and is sparse apparently. So the sparsifying transform for conventional CS-based image reconstructions will be no more a requisite for RRL1. And then the sparsity basis Ψ is an identity matrix. (2) It can been shown that any two row vectors of matrix A are approximately orthogonal, so that the system matrix A can be used as an approximately orthogonal measurement system Φ. Finally, the RRL1 method was designed to solve the constrained ℓ_1-norm minimization problem:

$$\min_X \|X\|_{l_1}, \quad s.t.\ \ AX = p \tag{4}$$

where X is $\partial\delta\,(x,y)/\partial x$ or $\partial\delta\,(x,y)/\partial y$, p is $\theta \sin\phi$ or $\theta \cos\phi$, and A is the system matrix.

2.2 Method

There exist many numerical methods to solve the constrained optimization problem defined in Eq. (4). We solve it using a heuristic strategy. (1) Eq. (4) says that there is a huge quantity of candidate images fitting the limited measurements, and we are attempting to find the *best* candidate that minimizes the function $\|X\|_{l_1}$. (2) Obtaining an image that meets the constraint imposed by the measured projection data can be achieved via finding the solution of the ill-posed linear system of equations $AX = p$. (3) So we can use such an iterative computation scheme to get the *best* candidate that consists of two steps in each iteration: solving the linear system $AX = p$ and then minimizing the objective function $\|X\|_{l_1}$. The realization of the RRL1 method is a nested loop, whose pseudo code is presented in Fig. 2.

```
//Initialzation.
iter0, iter1, iter2;   //Iteration times.
h = 0;      //Step size of SD.
k = 0;
X^(k) = 0;   //Target image.
//RRL1 iterative reconstruction.
Do
{    //1. RR-module.
     j = 0;
     X̃_1^(j) = X^(k);
     Do
     {    Projection;
          Difference;
          Normalization;
          Back-projection;
          Correction;
          j = j+1
     }while( j ≤ iter1 )
     d = ‖X̃_1^(j-1) - X̃_1^(0)‖_{l_2};   //Balancing.
     (continue.....)
     //2. L1-module.
     X̃_2^(0) = X̃_1^(j-1);
     j = 0;
     Do
     {    ‖X̃_2^(j)‖_{l_1};   //Objective function.
          p^(j);      //Search direction.
          X̃_2^(j+1) = X̃_2^(j) + d·h·p^(j);
          j = j+1;
     }while( j ≤ iter2 )
     k = k+1;
     X^(k) = X̃_2^(j-1);
}while( j ≤ iter0 )
```

Fig. 2: Pseudo code of the RRL1 method

The inner loop includes two modules. RR-module solves the system $AX = p$ and L1-module minimizes the function $\|X\|_{l_1}$ by Steepest Descent (SD) technique. Intuitively, RR-module produces a candidate image that fits the measurements approximately, and then L1-module tries to find the *best* image by taking the candidate one as its initial guess. A factor d is introduced to maintain a numerical balance between two modules. Parameter h is the conventional step size of SD technique, which together with the factor d determines jointly the descent amplitude of the objective function.

Solving the ill-posed linear system. From a mathematic point of view, traditional iterative image reconstruction techniques actually are iterative numerical methods to solve an undetermined ill-posed linear system. Particularly, all these algorithms have a closed loop pipe-line structure as follows: {Proj >> Diff >> BP >> Corr}, where Proj and BP represent the projection and back-projection operations respectively, Diff says acquiring the *difference* between the original measurement and the projection of a reconstructed image, and Corr means correcting the reconstructed image according to the *difference* obtained in the Diff step. Divergences between their implementations are the definition of the *difference* and the correction

strategy. Starting with such a common algorithmic framework, RR-module solves the underdetermined ill-posed linear system approximately, using the following iterative computation scheme: {Proj >> Diff >> Norm >> BP >> Corr}, where Norm indicates a normalization manipulation onto the results of the Proj and Diff steps. This manipulation is to guarantee the consistency of the data and the numerical stability of the iterative computation. The Proj and BP operations in RR-module are distance-driven (it will be described next). And the *difference* in RR-module just is defined as deviation; and the correction strategy used by RR-module is conducting plus operation.

As mentioned above, the approximation solution of $AX = p$ produced by RR-module flows into L1-module and is used as an initial estimate of the target image X by SD technique. The task performed by RR-module also is referred to as rough-reconstruction in this paper.

Distance-driven projection and back-projection. The distance-driven method has lower arithmetic complexity, higher numerical accuracy and sequential memory access pattern, and can avoid the artefacts characteristics of ray-driven back-projection and pixel-driven projection [13]. So the RRL1 method uses the distance-driven strategy for the projection and back-projection operations in its RR-module. We also utilize the distance-driven back-projection to implement the FBP method and name it as DDFBP. DDFBP will be used to conduct the quantitive performance comparison between RRL1 and FBP in the experiments.

The reconstructed phase-contrast image. We have stated that the target phase-contrast image reconstructed by the RRL1 method is $\partial\delta(x,y)/\partial x$ or $\partial\delta(x,y)/\partial y$, and $\theta\sin\phi$ or $\theta\cos\phi$ serves as the projection data. In other words, RRL1 will generate the phase-contrast image of $\partial\delta(x,y)/\partial x$ when the data $\theta\sin\phi$ is input, while the image of $\partial\delta(x,y)/\partial y$ will be yielded once the data $\theta\cos\phi$ enters. As a whole, the RRL1 method is capable of reconstructing the spatial distribution of the refractive index decrement gradient (i.e., $\nabla\delta = (\partial\delta/\partial x, \partial\delta/\partial y)$), since we can acquire the phase-contrast gradient image according to the following equation:

$$|\nabla\delta| = \sqrt{|\partial\delta(x,y)/\partial x|^2 + |\partial\delta(x,y)/\partial y|^2} \tag{5}$$

In short, in order to reconstruct a phase-contrast gradient image, we need to apply the RRL1 method two times depending on the input data.

3 Experiments

The real data experiments presented here are to verify the performance of the RRL1 method when the parallel-beam projection is undersampled and noisy. It also involves the quantitive performance comparison with the analytic DDFBP method. Three sampling patterns will be involved in the experiments: (1) 36 views pattern - the source rotates at a step of 5.0 degrees over 0 to 180 degrees, (2) 90 views pattern - rotational step 2.0 degrees over 0 to 180 degrees, and (3) 180 views pattern - rotational step 1.0 degrees over 0 to 180 degrees. These three sampling patterns are considered being undersampled in this paper.

3.1 Data Acquisition

The real data was acquired at the High Energy Accelerator Research Organization (KEK, Japan), using their Bragg- and Laue-case analyzer based Dark Field Imaging (DFI) system. The monochro-

matic synchrotron X-ray beam at 35 keV is expanded to a square parallel beam by an asymmetrical Bragg-case monochromator collimator to cover the full object width. Pixel size of the CCD detectors is 29.6 microns. Projections were acquired at 0.5 degrees angular step over a full range of 0 to 180 degrees, producing a total of 360 projecions. Number of bins in each projection view is 450 and the height of data is 500 (i.e., the data size of each projection view is 500×450). The refraction angle data was estimated in a pre-processing step from the diffraction and the forward diffraction images using rocking curve fitting with polynomial functions [14]. The data were generated using a physical phantom dedicated to the investigation of contrast resolution of the KEK's DFI system. The phantom is an acrylic cylinder with 13 channels. Each channel is filled with water, ethanol or glycerin.

3.2 Tomographic Image Reconstruction

The refraction angle data is pre-processed first to get the applicable projection data $\theta \sin\phi$ or $\theta \cos\phi$. Then RRL1 or DDFBP method reconstructs the target images of $\partial\delta(x,y)/\partial x$ or $\partial\delta(x,y)/\partial y$ from $\theta \sin\phi$ or $\theta \cos\phi$. Finally, the reconstructed gradient image is obtained using Eq. (5). We demonstrate next the reconstruction result of the data set that is from the slice at data height 0 (i.e., *slice 0*). Fig. 3 (a)-(c) show the reconstructed gradient images of *slice 0* under the three sampling patterns, respectively by RRL1 or DDFBP method. The reconstructed image size is 450×450. The parameters $iter0$, $iter1$ and $iter2$ within RRL1's pseudo code are 2, 5 and 5 respectively.

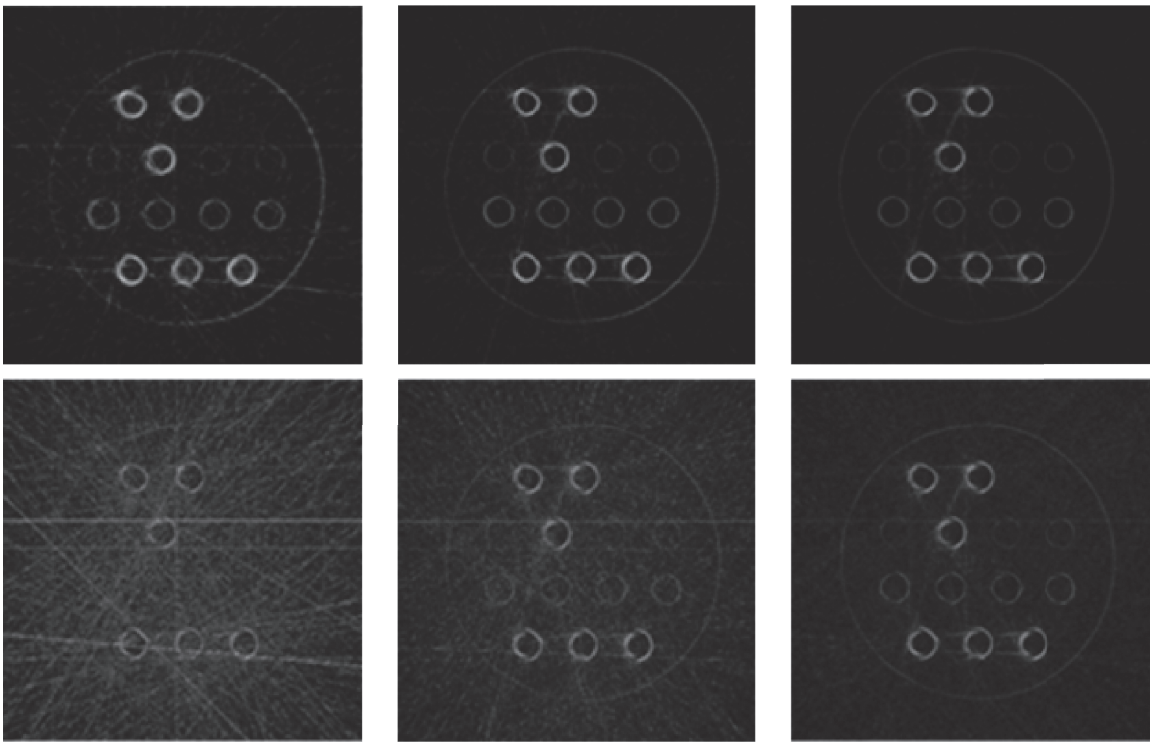

(a) (b) (c)

Fig. 3: The tomographic image reconstruction for *slice 0*. The top three images are the reconstructed gradient images by RRL1, and the bottom three are those by DDFBP. (a) 36 views pattern. (b) 90 views pattern. (c) 180 views pattern

3.3 Performance Comparison

Except for adopting common Peak Signal-to-noise Ratio (PSNR) indexes to evaluate the image quality, we also computed Universal Quality Index (UQI) [15] to assess the similarity between the reference and the reconstructed images. UQI index is defined as

$$UQI = \left(\frac{2\mu\mu_r}{\mu^2+\mu_r^2}\right)\left(\frac{2Cov(f,f^r)}{\sigma^2+\sigma_r^2}\right) \tag{6}$$

where μ_r and μ represent the mean pixel values of the two images , σ_r and σ are the standard deviations of them, and $Cov(f, f^r)$ is their covariance. It can be shown that the closer a reconstructed image to the reference one, the higher the quantity of UQI. UQI criterion reaches its maximum value 1.0 when the reconstructed image is identical to the reference one.

The actual tomographic image is unknown for the real data experiment. We suppose the data set of the 360 views sampling pattern (i.e., the source rotates at a step of 0.5 degrees over 0 to 180 degrees) is completed; and we use the reconstructed gradient image by the RRL1 method under this sampling pattern as the reference image for the calculation of PSNR and UQI. The results show the superiority of the RRL1 method over FBP evidently. Fig. 4 presents the graphical comparison between RRL1 and DDFBP of PSNR and UQI for *slice 0*.

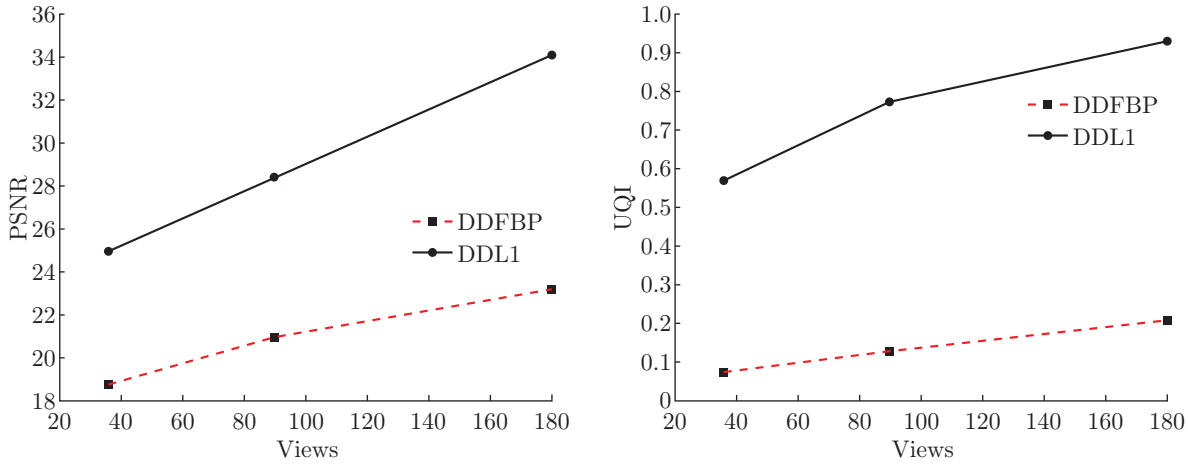

Fig. 4: The comparison of PSNR and UQI criteria between RRL1 and DDFBP for *slice 0*. (*left*: PSNR, *right*: UQI)

4 Discussions and Conclusion

We believe that the RRL1 method performs better than analytic FBP phase-contrast image reconstructions, particularly when the projection data is undersampled and noisy. Fig. 3 and 4 has indicated apparently that: (1) Either the reconstructed images produced by DDFBP or those by RRL1, the image quality will degrade with the reduction in number of projection views; (2) But for the images produced by DDFBP, their image qualities decrease dramatically with the views lessened, while the qualities of the images by RRL1 degrade less; (3) When the projection views reduced to a very small quantity (e.g., the 36 views sampling pattern), streak artefacts arise for the FBP reconstruction due to the violation of the Nyquist sampling theorem, even it goes

so far as to the desired image may be neglected; while the RRL1 method still yield tomographic images with satisfactory fidelity. As the undersampling CT scanning is a straight route to lower radiation dose or to shorten the data acquisition time, we think the RRL1 method shows potential for X-ray DPCT facilities in low dose tomography and fast acquisition imaging.

A new iterative image reconstruction method for X-ray DPCT is established using CS theory. The proposed method reconstructs the phase-contrast tomographic image of the refractive index decrement gradient from the refraction angle data with acceptable image quality even when the projection data is undersampled and noisy. This method is accurate and practical and outperforms the analytic FBP reconstruction, and shows potential for X-ray DPCT facilities in low dose tomography and fast acquisition imaging.

References

[1] C. David, B. Nohammer, H. H. Solak, E. Ziegler, Differential X-ray phase contrast imaging using a shearing interferometer, Appl. Phys. Lett., 81, 2002, 3287-3289

[2] F. Pfeiffer, M. Bech, O. Bunk, P. Kraft, E. F. Eikenberry, C. H. Bronnimann, C. Grunzweig, C. David, Hard-X-ray dark-field imaging using a grating interferometer, Nat. Mater., 7, 2008, 134-137

[3] I. Zanette, M. Bech, A. Rack, G. Le Duc, P. Tafforeau, C. David, J. Mohr, F. Pfeiffer, T. Weitkamp, Trimodal low-dose X-ray tomography, Proc. Natl. Acad. Sci., USA, 109, 2012, 10199-10204

[4] A. Bravin, P. Coan, P. Suortti, X-ray phase-contrast imaging: From pre-clinical applications towards clinics, Phys. Med. Biol., 58, 2013, R1-R35

[5] D. L. Donoho, Compressed sensing, IEEE Trans. Inform. Theory, 52, 2006, 1289-1306

[6] Y. Tsaig, D. L. Donoho, Extensions of compressed sensing, Signal Processing, 86, 2006, 549-571

[7] G. H. Chen, J. Tang, S. Leng, Prior image constrained compressed sensing (PICCS): A method to accurately reconstruct dynamic CT images from highly undersampled projection data sets, Med. Phys., 35, 2008, 660-663

[8] E. Y. Sidky, X. Pan, Image reconstruction in circular cone-beam computed tomography by constrained, total-variation minimization, Phys. Med. Biol., 53, 2008, 4777-4807

[9] G. Wang, Y. Bresler, V. Ntziachristos, Compressive sensing for biomedical imaging, IEEE Trans. Med. Imaging, 30, 2011, 1013-1016

[10] Q. Xu, E. Y. Sidky, X. Pan, M. Stampanoni, P. Modregger, M. A. Anastasio, Investigation of discrete imaging models and iterative image reconstruction in differential X-ray phase-contrast tomography, Opt. Express, 20, 2012, 10724-10749

[11] W. Cong, J. Yang, G. Wang, Differential phase-contrast interior tomography, Phys. Med. Biol., 57, 2012, 2905-2914

[12] T. J. Davis, D. Gao, T. E. Gueyev, A. W. Stevenson, S. W. Wilkins, Phase-contrast imagimg of weakly absorbing materials using hard X-rays, Nature, 373, 1995, 595-597

[13] B. D. Man, S. Basu, Distance-driven projection and backprojection in three dimensions, Phys. Med. Biol., 49, 2004, 2463-2475

[14] N. Sunaguchi, T. Yuasa, Q. Huo, Ichihara Shu, M. Ando, X-ray refraction-contrast computed tomography images using dark-field imaging optics, Appl. Phys. Lett., 97, 2010, 153701-153703

[15] Z. Wang, A. C. Bovik, H. R. Sheikh, E. P. Simoncelli, Image quality assessment: From error visibility to structural similarity, IEEE Trans. Image Process, 13, 2004, 600-612